Brain tissue types resolved using spherical deconvolution of multi-shell diffusion MRI data

Ben Jeurissen[1], Jacques-Donald Tournier[2,3], Thijs Dhollander[4], Alan Connelly[2,5], and Jan Sijbers[1]

[1]iMinds-Vision Lab, University of Antwerp, Antwerp, Belgium, [2]The Florey Institute of Neuroscience and Mental Health, Melbourne, Victoria, Australia, [3]Division of Imaging Sciences & Biomedical Engineering, King's College London, London, United Kingdom, [4]Medical Imaging Research Center, KU Leuven, Belgium, [5]The Florey Department of Neuroscience, University of Melbourne, Victoria, Australia

Target audience: Researchers who want to perform spherical deconvolution of diffusion-weighted (DW) MRI data acquired at multiple shells in q-space.

Introduction: Constrained spherical deconvolution (CSD) has become one of the most widely used methods to extract white matter (WM) fibre orientation information from DW MRI data, overcoming the crossing fibre limitations inherent in the diffusion tensor model [1]. CSD is already being routinely used to obtain high quality fibre orientation distribution function (fODF) estimates and fibre tractograms [2]. However, there are currently some limitations that have yet to be addressed. First, CSD typically only supports data acquired on a single shell in q-space. For multi-shell data sets, users are forced to use just the outer shell, discarding potentially valuable information from the inner shells. With multi-shell data becoming more and more prevalent, there is a growing need for CSD to fully support such data. Second, CSD can provide high quality fODF estimates in voxels containing WM *only*. In voxels containing other tissue types such as grey matter (GM) and cerebrospinal fluid (CSF), the WM response function may no longer be valid and spherical deconvolution produces unreliable, noisy fODF estimates [3]. While multiple tissue types cannot be distinguished from single shell data, the unique multi-shell decay curves of the different tissue types may provide an opportunity to tease out the contributions from each tissue. The aim of this study is to incorporate support for multi-shell data into the CSD approach and to exploit multi-shell data to estimate a multi-tissue ODF.

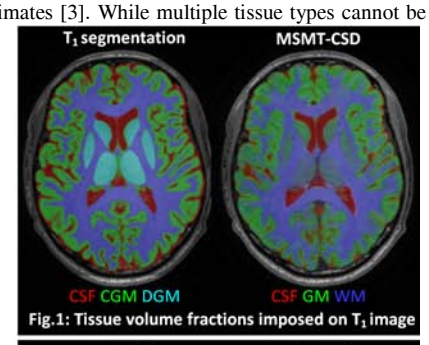

Fig.1: Tissue volume fractions imposed on T_1 image

Methods: *Acquisition*: DW data were acquired on a 3T scanner, using an 8-channel receiver head coil. Diffusion weightings of b = 0, 700, 1200 and 2800 s/mm^2 were applied in 5, 25, 45 and 75 directions, respectively. In addition, 5 b = 0 s/mm^2 images were acquired with reversed phase encoding, for the purpose of EPI correction [4]. Other imaging parameters were: TR/TE: 9500/100 ms; voxel size: 2×2×2 mm^3; matrix: 120×120; slices: 68; NEX: 1. A 1×1×1 mm^3 T_1-weighted anatomical image was also acquired, to aid identification of the different tissue types. *Post-processing*: DW images were corrected for motion and eddy current distortions [5] and for EPI distortions [4], to ensure proper alignment of the DW images to each other and to the anatomical data. Four tissue types (CSF, cortical GM (CGM), deep GM (DGM) and WM) were segmented on the anatomical image as outlined in [6]. *ODF estimation*: CSD can be formulated as a constrained linear least squares problem of the form: $\hat{x} = \min_x \|C \cdot x - d\|_2^2$ s.t. $A \cdot x \geq 0$, where C is the spherical convolution matrix relating the vector of unknown WM fODF spherical harmonic (SH) coefficients, x, to the vector of measured DW signal intensities, d, and A is the constraint matrix relating the WM fODF SH coefficients x to their amplitudes. We will refer to this approach as *'single-shell, single-tissue CSD'* (SSST-CSD). The above framework can be extended to support both multiple shells and multiple tissue types as follows: $\begin{bmatrix}\hat{x}_{\mathrm{CSF}}\\ \hat{x}_{\mathrm{GM}}\\ \hat{x}_{\mathrm{WM}}\end{bmatrix} = \min_{\substack{x_{\mathrm{CSF}}\\ x_{\mathrm{GM}}\\ x_{\mathrm{WM}}}} \left\| \begin{bmatrix} C_{1,\mathrm{CSF}} & C_{1,\mathrm{GM}} & C_{1,\mathrm{WM}} \\ \vdots & \vdots & \vdots \\ C_{n,\mathrm{CSF}} & C_{n,\mathrm{GM}} & C_{n,\mathrm{WM}} \end{bmatrix} \cdot \begin{bmatrix} x_{\mathrm{CSF}} \\ x_{\mathrm{GM}} \\ x_{\mathrm{WM}} \end{bmatrix} - \begin{bmatrix} d_1 \\ \vdots \\ d_n \end{bmatrix} \right\|_2^2$ s.t. $\begin{bmatrix} A_{\mathrm{CSF}} & 0 & 0 \\ 0 & A_{\mathrm{GM}} & 0 \\ 0 & 0 & A_{\mathrm{WM}} \end{bmatrix} \cdot \begin{bmatrix} x_{\mathrm{CSF}} \\ x_{\mathrm{GM}} \\ x_{\mathrm{WM}} \end{bmatrix} \geq 0$, where $C_{i,t}$ is the spherical convolution matrix relating the vector of unknown ODF SH coefficients of tissue t, x_t, to the vector of DW signal intensities measured on the i-th shell, d_i; and A_t is the matrix relating the ODF SH coefficients of tissue t to their amplitudes. We will refer to this approach as *'multi-shell, multi-tissue CSD'* (MSMT-CSD). In this study, both the WM fODFs (x and x_{WM}) are assumed to be anisotropic with $l_{\max} = 8$ (45 coefficients). The CSF and GM ODFs (x_{CSF} and x_{GM}) are assumed to be isotropic with $l_{\max} = 0$ (1 coefficient each). C and $C_{i,\mathrm{WM}}$ are estimated from the data by averaging reoriented DW signals from voxels containing a single, clearly defined fibre orientation (FA > 0.7) [1]. $C_{i,\mathrm{CSF}}$ and $C_{i,\mathrm{GM}}$ are estimated by averaging DW signals from voxels for which the four tissue segmentation reported the respective volume fraction to be > 95%. $A = A_{\mathrm{WM}}$, is a matrix transforming the WM fODF SH coefficients into their corresponding amplitudes along a set of 300 uniformly distributed orientations, imposing positivity of the WM fODF [1]. A_{CSF} and A_{GM} are each a scalar 1, imposing positivity of the volume fractions.

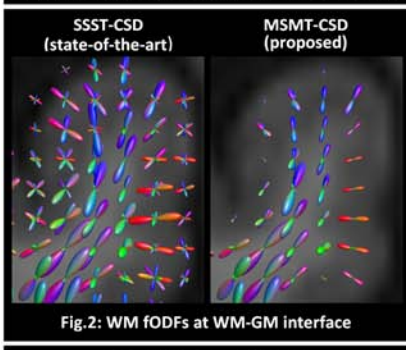

Fig.2: WM fODFs at WM-GM interface

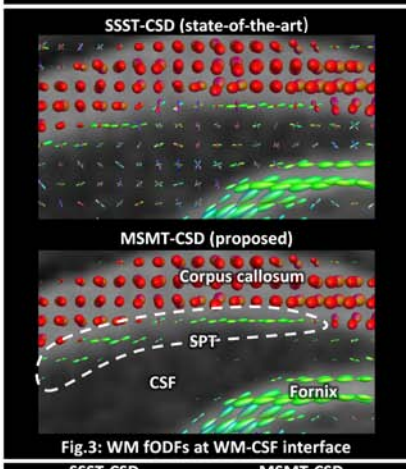

Fig.3: WM fODFs at WM-CSF interface

Results: Fig. 1 shows the tissue volume fraction maps estimated with MSMT-CSD alongside those obtained by segmenting the anatomical image. Note the high correlation between both maps. In DGM, MSMT-CSD typically reports a mixture between GM and WM, which is consistent with anatomical knowledge about the DGM. Fig. 2 shows fODFs extending into a gyrus of the cerebral cortex estimated by SSST-CSD and MSMT-CSD. The SSST-CSD solution exhibits spurious lobes at the WM-GM interface. The MSMT-CSD solution provides nearly identical results in pure WM voxels. However, at the WM-GM interface, fODF estimates are markedly improved, showing a strong reduction in spurious lobes and an increase in the consistency of the true fODF lobes. Fig. 3 shows fODFs near the ventricles estimated by SSST-CSD and MSMT-CSD. As before, MSMT-CSD strongly reduces spurious lobes and increases the consistency of the true fODF lobes at the interface and leaves the pure WM fODFs unchanged. Note also how MSMT-CSD cleanly recovers the WM fibres of the septum pellucidum (SPT). SPT is made up of a mixture of WM and GM and is very hard to resolve cleanly at 3 T, due to partial volume effects with its own GM and nearby CSF [7]. Fig. 4 shows a sagittal slab visualisation of a whole brain probabilistic tractogram calculated from both SSST-CSD and MSMT-CSD fODFs using an fODF amplitude threshold of 0.03 [8]. At such low threshold, SSST-CSD produces many spurious fibres near the tissue interfaces, which are not present in the MSMT-CSD solution.

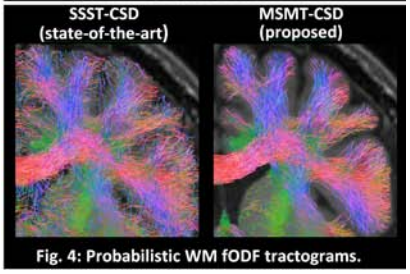

Fig. 4: Probabilistic WM fODF tractograms.

Discussion: We have shown that it is plausible to simultaneously estimate ODFs from different tissue types using multi-shell DW data. The MSMT-CSD has two distinctive features compared to SSST-CSD. First, it produces a map of the WM/GM/CSF volume fractions, directly from the DW data. The ability to estimate tissue volume fractions directly from the DW data can potentially relax the acquisition requirements for anatomically constrained tractography [6], which uses these as a biological prior for fibre tractography. Second, it produces much more reliable WM fODF estimates at the interfaces with GM and CSF. This results in more anatomically plausible WM fibre tractography in regions throughout the brain. It also allows tractography to be performed with significantly lower fODF thresholds, increasing the sensitivity to detect small fibre bundles that could go undetected with conventional thresholds.

References: [1] Tournier et al., NeuroImage 35(4):1459-1472, 2007; [2] Farquharson et al., J Neurosurg 118(6):1367-1377, 2013; [3] Dell'acqua et al., NeuroImage 49(2):1446-1458, 2010; [4] Andersson et al., NeuroImage 20(2):208-219, 2004; [5] Raffelt et al., NeuroImage 59(4):3976-3994, 2012; [6] Smith et al., NeuroImage 62(3):1924-1938, 2012; [7] Cho et al., World Neurosurg, DOI:10.1016/j. wneu.2013.08.022, in press; [8] Tournier et al., Int J Imaging Syst Technol 22(1):53-66, 2012.